Proceedings of the 7th International Symposium on Cavitation
CAV2009
August 17-22, 2009, Ann Arbor, Michigan, USA

CAV2009 – Paper No. 132

Dynamics of a vapor bubble near a thin elastic plate

M. T. Shervani-Tabar
Department of Mechanical Engineering, University of Tabriz, Tabriz, Iran

M. R. Shabgard
Department of Manufacturing, University of Tabriz, Tabriz, Iran

M. Rezaee
Department of Mechanical Engineering, University of Tabriz, Tabriz, Iran

R. Zabihyan
Member of scientific association; Azad University, Tabriz branch, Tabriz, Iran

ABSTRACT

Numerical and experimental results show that during the collapse phase of a vapor bubble near a rigid boundary, in the absence of strong buoyancy forces, a liquid micro jet is developed on the side of the bubble far from the rigid surface and directed towards it. Numerical and experimental results also show that, in the case of a bubble near a free surface, during the collapse phase of the bubble and in the absence of strong buoyancy forces, the vapor bubble is repelled by the free surface. In this case a liquid micro jet is developed on the closest side of the bubble to the free surface and is directed away from it. The dynamic behavior of a vapor bubble near a free surface leads to the idea that a vapor bubble during its growth and collapse phases near a deformable diaphragm may have a behavior similar to its behavior near a free surface.
In this paper dynamics of a vapor bubble during its growth and collapse phases near a thin elastic plate is investigated. It has been shown that the growth and collapse of a vapor bubble generated due to a high local energy input causes considerable deformation on the nearby thin elastic plate.
Different thin elastic plates with different thicknesses and different flexural rigidities are assumed and the dynamic behavior of a vapor bubble near each of these plates is investigated. Results show that during the growth and collapse of a vapor bubble near a thin elastic plate with a proper thickness and flexural rigidity, in the absence of strong buoyancy forces, a liquid micro jet may develop on the closest side of the bubble to the thin elastic plate and directed away from it.

INTRODUCTION

Experimental and numerical investigations on the dynamic behavior of a vapor bubble near deformable surfaces have been carried out by some researchers. These investigations show that during the collapse phase of a vapor bubble near a deformable surface, in the absence of strong buoyancy forces, the minute displacement of the deformable surface may cause the liquid micro jet to be directed away from it [1-7]. In an important study, Duncan and Zhang [8] investigated the dynamics of a collapsing cavity near a compliant wall numerically. They noted that when the wall is rigid, the generated liquid jet during collapse phase is directed towards the boundary but near an elastic membrane the liquid jet may be directed away from the membrane. In their research, they assumed that the vapour bubble, initially, is in its maximum size. This is because of the fact that, in the case of a vapour bubble initially in its minimum size, the pressure distribution on the nearby boundary changes very fast. Consequently, the iteration scheme which is employed by Duncan and Zhang [8] for evaluating of initial pressure distribution on the compliant wall does not work any more. In the present paper, theory of explosion bubble which is developed by Best [9], is employed and in this case it is possible to simulate an explosion bubble growing from its initial minimum volume.

THEORY OF THE PROBLEM

In this paper dynamics of a vapor bubble generated by a high local energy input near a thin elastic plate is investigated. The used samples are Steel, Aluminum and Magnesium. The physical characteristics of the plates have been shown in the Table.1. The generated vapor bubble is located in the midpoint and below of the thin plate. In the all cases the standoff parameter, γ, is equal to 1. The initial pressure inside the vapor bubble is very high and is related to the initial size of the bubble. Figure 1 shows the initial position of the bubble and the metal plate.

It is assumed that the generated vapor bubble contains a mixture of non-condensable and non-chemically reacting gas and saturated vapor. The non-condensable gas inside the vapor bubble is assumed to be an ideal gas. Therefore the pressure inside the bubble is obtained by summation of the partial pressures of the saturated vapor and the ideal gas. It is obvious that the partial pressure of the ideal gas inside the bubble is the dominant pressure and is obtained by the isentropic relation between the pressure inside the bubble and the bubble volume.

According to Best [9] in the case of an explosion vapor bubble with an initial small radius, R_0, the bubble generated by a high local energy input contains a mixture of saturated vapor pressure and an ideal gas with a very high partial pressure. The vapor bubble is assumed to be spherical in its initial minimum volume. The equation of purely radial motion of a bubble generated by a high local energy input is given as:

$$R\ddot{R} + \frac{3}{2}\dot{R}^2 + \frac{P_\infty - P_b}{\rho} = 0 \qquad (1)$$

Where P_b is the variable pressure inside the bubble. P_∞ is the pressure in the far field and *R* is the radius of the bubble, with dots denoting time derivatives

For obtaining governing equation of the hydrodynamic behavior of the liquid domain around the vapor bubble, it is assumed that the liquid is incompressible, inviscid, and irrotational and surface tension is neglected. In this case the flow of the liquid around the vapor bubble is a potential flow. Therefore the Green's integral formula is the governing equation of the flow around the vapor bubble and is given as:

$$C(p)\phi(p) + \int_S \phi(q)\frac{\partial}{\partial n}\left[\frac{1}{|p-q|}\right]dS = \int_S \frac{\partial}{\partial n}[\phi(q)]\left(\frac{1}{|p-q|}\right)dS \qquad (2)$$

Where S is the boundary of the liquid domain, ϕ is the velocity potential and $\frac{\partial\phi}{\partial n}$ is the normal velocity of the boundary. P is any point in the liquid domain, Ω, or on the boundary, S, and q is any point on the boundary, S.

$$C(p) = 2\pi \; ; \quad if \;\; P \in S$$

And

$$C(p) = 4\pi ; \quad if \;\; P \in \Omega$$

The unsteady Bernoulli equation in its Lagrangian form is used for calculating velocity potential at the successive time steps and is given as:

$$\frac{D\phi}{Dt} = \frac{p_\infty - p_b}{\rho} + \frac{1}{2}|\nabla\phi|^2 \qquad (3)$$

The dynamic behavior of the elastic plate has been modeled by the axial symmetric equation of the motion of a thin circular plate with uniform thickness (Love [11]):

$$D\nabla^4 w(r,t) + \rho H\ddot{w}(r,t) = P(r,t) \qquad (4)$$

Where

$$D = \frac{EH^3}{12(1-\nu^2)} \qquad (5)$$

In equations (4) and (5), *w* is the vertical displacement of the plate, ρ is the mass per unit area, *H* is the thickness of the plate, *P* is the pressure on the surface of the plate and D is the flexural rigidity of the plate.

Also *E* is the elastic module of the plate and ν is the Poissons' ratio.

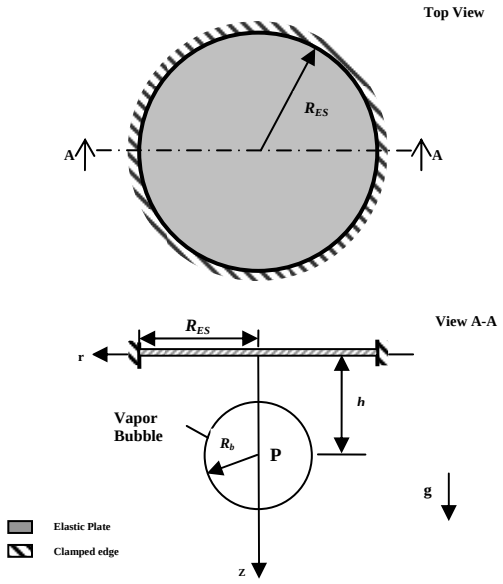

Figure 1: Schematic Representation of the elastic plate and the coordinate system and initial position of the bubble.

During the growth and collapse phases of the bubble, the vertical velocity on the surface of the elastic plate is equal to the vertical velocity of the nearby fluid. Thus on the interface of the flow and elastic plate it can be written that (Duncan et al [8]):

$$\begin{cases} \dfrac{\partial w}{\partial t} = \dfrac{\partial\phi}{\partial z} = \psi & z = 0 \\ p(r,t) = -\rho\dfrac{\partial\phi}{\partial t} + p_\infty & z = 0 \end{cases} \qquad (6)$$

NUMERICAL IMPLEMENTATION

In the numerical model the interface of the liquid domain and the surface of the plate are discretized by linear segments, the bubble boundary is discretized by cubic spline elements,

and the problem is axisymmetric. Collocation points are located at the mid point of each element. Velocity potential and its normal derivatives are assumed to be constant along each element. In fig. 2, z is the vertical axis and the radial axis is indicated by r. Also n is the normal velocity on the bubble boundary and g is the gravity acceleration.

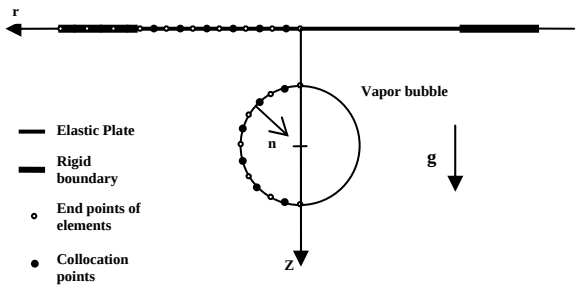

Figure 2: discretize of the bubble boundary and the interface of the liquid domain with surface of the Elastic plate

r and *z* for each element are expressed as:

$$\begin{cases} r_j^{i+1} = r_j^i + u_j \Delta t \\ z_j^{i+1} = z_j^i + v_j \Delta t \end{cases} \qquad (7)$$

Where u_j and v_j are the radial and vertical velocity of each element on the surface of the bubble, respectively. The superscript refers to the time steps and subscript refers to the nodes. To obtain accurate values of the u_j and v_j, the second-order Rung-Kutta method is used.

$$\begin{cases} u_j = \frac{1}{2}(u_j^i + u_j^{i+1}) \\ v_j = \frac{1}{2}(v_j^i + v_j^{i+1}) \end{cases} \qquad (8)$$

Equation (9) represents the discretized form of unsteady Bernoulli equation and allows the velocity potential to be time marched over a time increment of Δt.

$$\phi_j^{i+1} = \phi_j^i + \Delta t \left\{ \frac{p_\infty - p_b}{\rho} + \frac{1}{2}\left|\nabla \phi\right|^2 \right\} \qquad (9)$$

The equation of the motion of the plate (4) is decomposed into two first-order differential equations with respect to time:

$$\frac{\partial w}{\partial t} = \psi , \qquad (10)$$

$$\frac{\partial \psi}{\partial t} = \frac{P(r,t)}{\rho H} - \frac{D}{\rho H}\nabla^4 w \qquad (11)$$

The predictor-corrector scheme is used to discretize these equations:

Predictor step:

$$\begin{Bmatrix} \overline{w}_j^{i+1} \\ \overline{\psi}_j^{i+1} \end{Bmatrix} = \begin{Bmatrix} w_j^i \\ \psi_j^i \end{Bmatrix} + (t_{i+1} - t_i) \begin{Bmatrix} \psi_j^i \\ \left[\frac{\partial \psi}{\partial t}\right]_j^i \end{Bmatrix}, \qquad (12)$$

Corrector step:

$$\begin{Bmatrix} w_j^{i+1} \\ \psi_j^{i+1} \end{Bmatrix} = \begin{Bmatrix} w_j^i \\ \psi_j^i \end{Bmatrix} + \frac{1}{2}(t_{i+1} - t_i) \begin{Bmatrix} \psi_j^i + \overline{\psi}_j^{i+1} \\ \left[\frac{\partial \psi}{\partial t}\right]_j^i + \left[\frac{\partial \overline{\psi}}{\partial t}\right]_j^{i+1} \end{Bmatrix}, \qquad (13)$$

Where

$$\left[\frac{\partial \psi}{\partial t}\right]_j^i = \frac{P(r_j, t_i)}{\rho H} - \frac{D}{\rho H}\left[\left(\frac{\partial^2}{\partial r^2} + \frac{1}{r}\frac{\partial}{\partial r}\right)^2 w\right]_j^i ,$$

and

$$\left[\left(\frac{\partial^2}{\partial r^2} + \frac{1}{r}\frac{\partial}{\partial r}\right)^2 w\right]_j^i =$$

$$\begin{cases} \left(\frac{1}{\Delta r^4} + \frac{1}{r\Delta r^3}\right)w_{j+2}^j - \left(\frac{4}{\Delta r^4} + \frac{2}{r\Delta r^3} + \frac{1}{r^2\Delta r^2} - \frac{1}{2r^3\Delta r}\right)w_{j+1}^j + \\ \left(\frac{6}{\Delta r^4} + \frac{2}{r^2\Delta r^2}\right)w_j^j - \left(\frac{4}{\Delta r^4} - \frac{2}{r\Delta r^3} + \frac{1}{r^2\Delta r^2} + \frac{1}{2r^3\Delta r}\right)w_{j-1}^j + & 0 < r_i < R_m \\ \left(\frac{1}{\Delta r^4} - \frac{1}{r\Delta r^3}\right)w_{j-2}^j & \\ \left(\frac{2}{\Delta r^4}\right)w_{j+2}^j - \left(\frac{8}{\Delta r^4} + \frac{2}{r^2\Delta r^2}\right)w_{j+1}^j + \left(\frac{6}{\Delta r^4} + \frac{2}{r^2\Delta r^2}\right)w_j^j & r_i = 0 \\ \left(\frac{2}{\Delta r^4}\right)w_{j-2}^j - \left(\frac{8}{\Delta r^4} + \frac{2}{r^2\Delta r^2}\right)w_{j-1}^j & r_i = R_m \end{cases}$$

In the above equations, Δr is the radial distance between nodes on the surface of the boundary and $\theta = \frac{\partial w}{\partial r} = 0$ at $r = 0$ and $r = R_{ES}$.

The discretizad form of equations (6) are:

$$\begin{cases} \left[\frac{\partial w}{\partial t}\right]_j^i = \left[\frac{\partial \phi}{\partial z}\right]_j^i = \psi_j^i \\ P_j^{i+1} - P_\infty = \rho \frac{\phi_j^{i+1} - \phi_j^i}{t_{i+1} - t_i} \end{cases} \qquad (14)$$

Equation (15) is a system of linear equations which represents the discretized form of equation (2).

$$2\pi\phi(P_i)+\sum_{j=1}^{M+2N}\left\{\phi(q_j)\int_{S_j}\frac{\partial}{\partial n}\left[\frac{1}{|p_i-q_j|}\right]dS\right\}= \sum_{j=1}^{M+2N}\left\{\frac{\partial}{\partial n}[\phi(q_j)]\int_{S_j}\left[\frac{1}{|p_i-q_j|}\right]dS\right\} \quad (15)$$

A variable time step is defined as:

$$\Delta t=\min\left|\frac{\Delta\phi}{\frac{p_\infty-p_c}{\rho}+\frac{1}{2}(\psi^2+\eta^2)}\right| \quad (16)$$

Where $\Delta\phi$ is some constant and represents the maximum increment of the velocity potential between two successive time steps. Also p_c is saturated vapour pressure, ψ is normal velocity on the boundary of the liquid domain and η is tangential velocity.

NON_DIMENSIONALISING OF THE PROBLEM

The problem is non-dimensionalised by employing the maximum radius of the bubble, R_m, the liquid density, ρ_l, the vapor density, ρ_V, the pressure in the far field, P_∞, and the saturated vapor pressure, p_c.

The main non-dimensional parameters are written on the nomenclature.

Table 1: Physical characteristics of the used samples

Sample	E (GPa)	$\rho\ kg/m^3$	ν
Steel	200	7860	0.29
Aluminum	70	2700	0.36
Magnesium	45	1800	0.35

RESULTS AND DISCUSSION

In all cases, stand-off parameter, γ, is equal 1 and the maximum radius of the bubble, the pressure in the far field and the saturated vapor pressure are assumed as:

$R_m=0.02m,\ P_\infty=300000\,Pa\ and\ P_c=2000\,Pa$.

Figures 3-5 illustrate the variation of the relative volume of the bubble (The ratio of volume of the bubble with respect to its minimum volume) against non-dimensional time when the growth and collapse phases of the bubble occurs near a thin elastic plate. In figure 3 the elastic plate is steel, while in figures 4 and 5 the elastic plate is aluminum and magnesium respectively. These figures show that by increasing the thickness of the elastic plate the maximum radius of the bubble to which the vapor bubble expands becomes smaller. These figures also show that by decreasing the thickness of the elastic plate the life time of the bubble increases. This is in contrast with the dynamics of a vapor bubble near a compliant coating. In the latter case the life time of the vapor bubble by increasing the compliancy of the coating decreases [8 and 12].

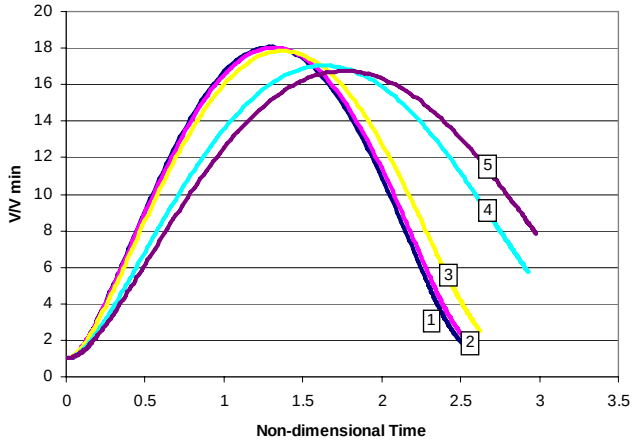

Figure 3: Variation of the bubble volume with respect to non-dimensional time for Steel sample in the cases of: (1) H*=0.005 (2) H*=0.0025 (3) H*=0.001 (4) H*=0.0004 (5) H*=0.00035

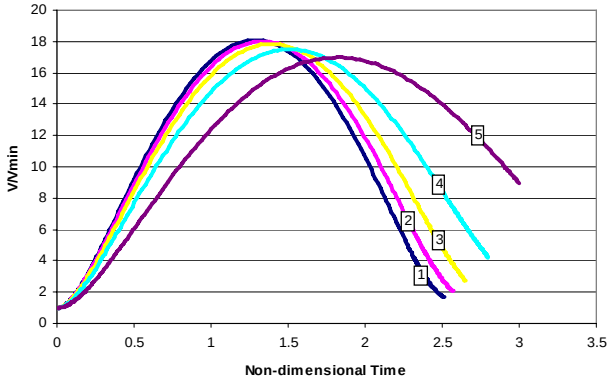

Figure 4: Variation of the bubble volume with respect to non-dimensional time for Aluminum sample in the cases of: (1) H*=0.05 (2) H*=0.005 (3) H*=0.0025 (4) H*=0.0015 (5) H*=0.001

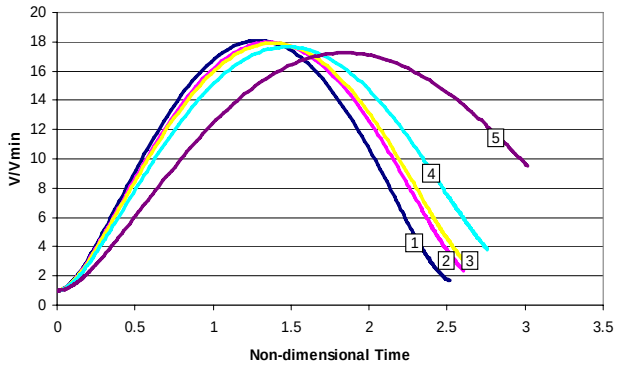

Figure 5: Variation of the bubble volume with respect to non-dimensional time for Magnesium sample in the cases of: (1) H*=0.05 (2) H*=0.005 (3) H*=0.004 (4) H*=0.0025 (5) H*=0.0015

Figures 6-8 show the movement of the bubble centroid in the cases of figures 3-5. These figures show that by decreasing the thickness of the thin metal plate the movement of the bubble centroid away from the thin metal plate increases.

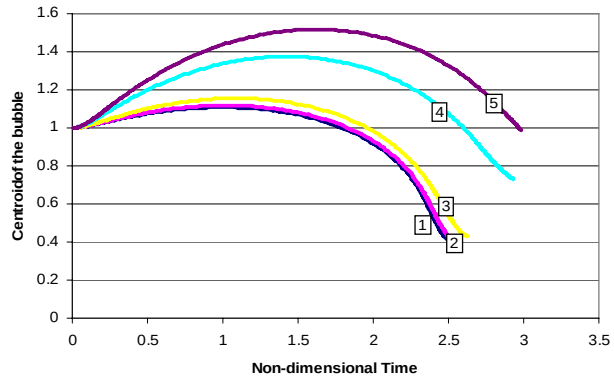

Figure 6: Variation of the centroid of the bubble with respect to non-dimensional time for Steel sample in the cases of: (1) H*=0.005 (2) H*=0.0025 (3) H*=0.001 (4) H*=0.0004 (5) H*=0.00035

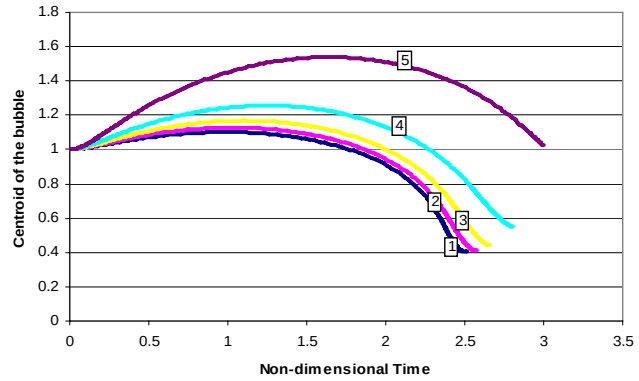

Figure 7: Variation of the centroid of the bubble with respect to non-dimensional time for Aluminum sample in the cases of: (1) H*=0.05 (2) H*=0.005 (3) H*=0.0025 (4) H*=0.0015 (5) H*=0.001

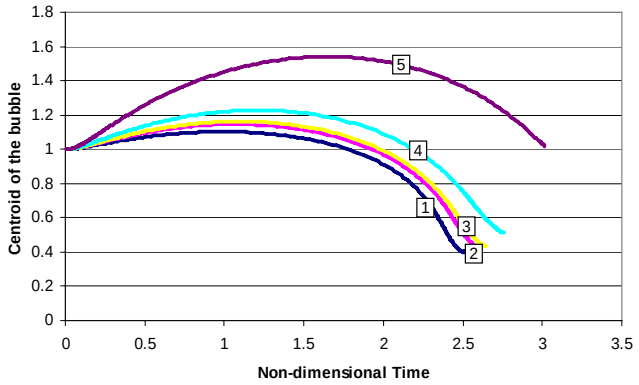

Figure 8: Variation of the bubble volume with respect to non-dimensional time for Magnesium sample in the cases of: (1) H*=0.05 (2) H*=0.005 (3) H*=0.004 (4) H*=0.0025 (5) H*=0.0015

Figures 9-11 illustrate the variation of the non-dimensional velocity of the far point of the bubble boundary from the elastic thin metal plate against non-dimensional time. This is the velocity of the liquid micro jet which is directed to the thin elastic plate. These figures show that by decreasing the thickness of the elastic metal plate the velocity of the liquid micro jet decreases.

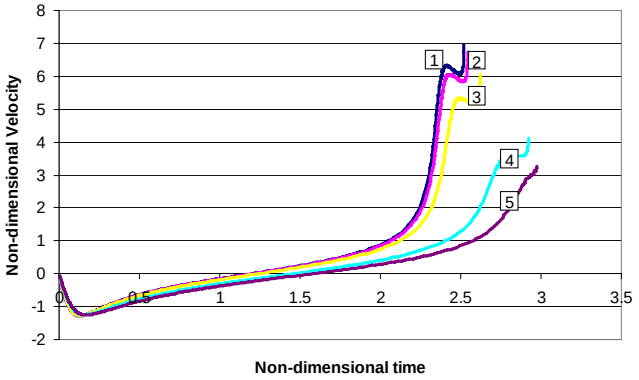

Figure 9: Velocity variation of the liquid jet on the bubble boundary far from the elastic plate with respect to non-dimensional time for Steel sample in the cases of: (1) H*=0.005 (2) H*=0.0025 (3) H*=0.001 (4) H*=0.0004 (5) H*=0.00035

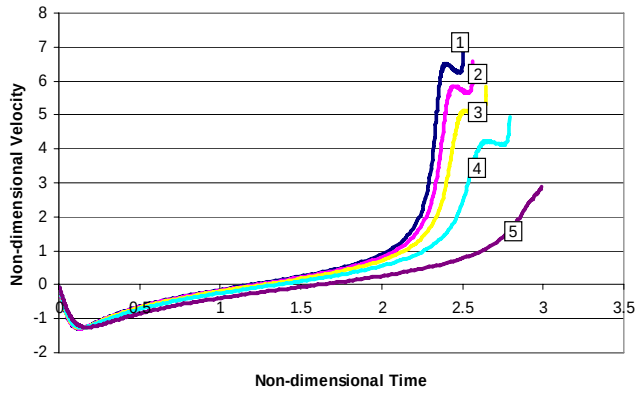

Figure 10: Velocity variation of the liquid jet on the bubble boundary far from the elastic plate with respect to non-dimensional time for Aluminum sample in the cases of: (1) H*=0.05 (2) H*=0.005 (3) H*=0.0025 (4) H*=0.0015 (5) H*=0.001

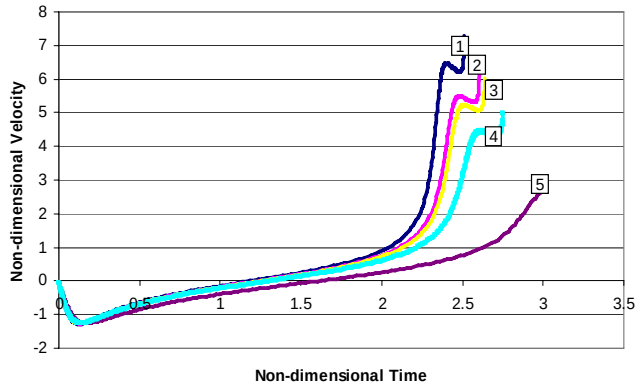

Figure 11: Velocity variation of the liquid jet on the bubble boundary far from the elastic plate with respect to non-dimensional time for Magnesium sample in the cases of: (1) H*=0.05 (2) H*=0.005 (3) H*=0.004 (4) H*=0.0025 (5) H*=0.0015

Figures 12-14 show the non-dimensional velocity of the elastic thin metal plate at its intersection with the vertical axis against non-dimensional time during the growth and collapse phases of the vapor bubble. These figures show that by decreasing the thickness of the thin elastic plate, the movement of the centre point of the plate increases.

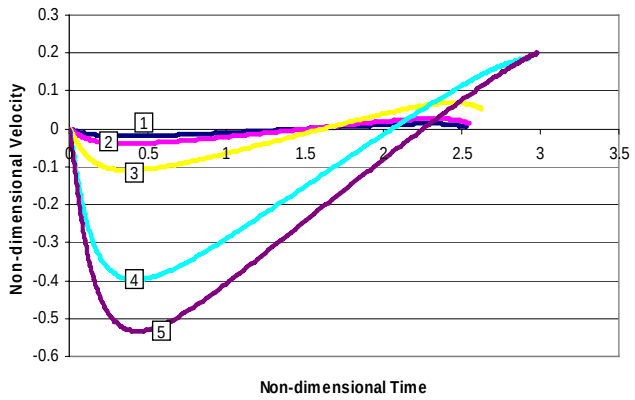

Figure 12: Vertical velocity of the Steel plate at r=0 versus non-dimensional time in the cases of: (1) H*=0.005 (2) H*=0.0025 (3) H*=0.001 (4) H*=0.0004 (5) H*=0.00035

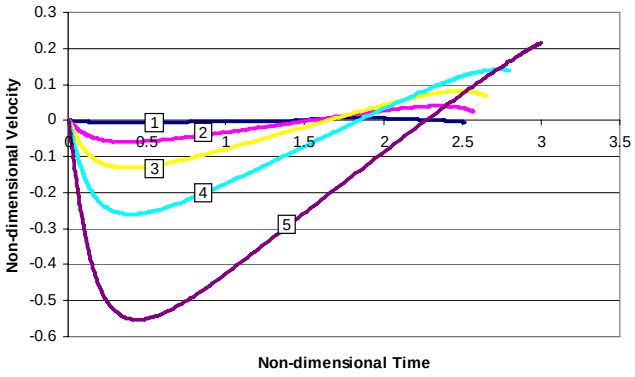

Figure 13: Vertical velocity of the Aluminum plate at r=0 versus non-dimensional time in the cases of: (1) H*=0.05 (2) H*=0.005 (3) H*=0.0025 (4) H*=0.0015 (5) H*=0.001

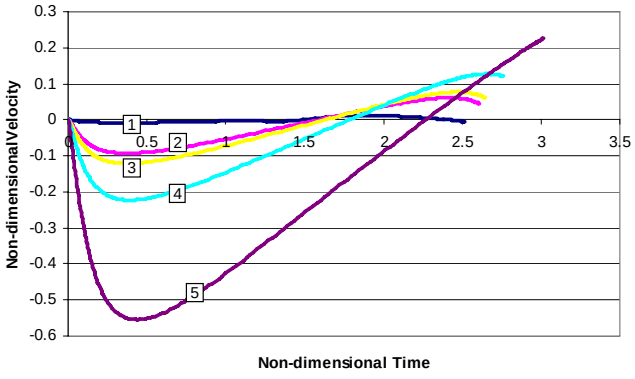

Figure 14: Vertical velocity of the Magnesium plate at r=0 versus non-dimensional time in the cases of: (1) H*=0.05 (2) H*=0.005 (3) H*=0.004 (4) H*=0.0025 (5) H*=0.0015

Figures 15, 16 and 17 illustrate the variation of the pressure on the intersection of vertical axis with different elastic thin metal plates against non-dimensional time. These figures show that by decreasing the thickness of the thin elastic plates, the pressure on the intersection of the vertical axis with different thin metal plates

at the end of the collapse phase and when the liquid micro jet pierces the opposite side of the bubble becomes lower.

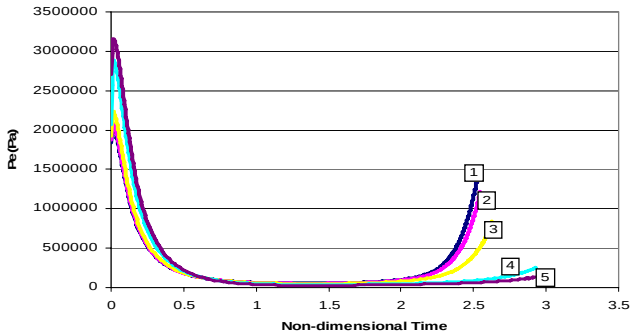

Figure 15: Pressure on the Steel plate surface at r=0 versus Non-dimensional time in the cases of: (1) H*=0.005 (2) H*=0.0025 (3) H*=0.001 (4) H*=0.0004 (5) H*=0.00035

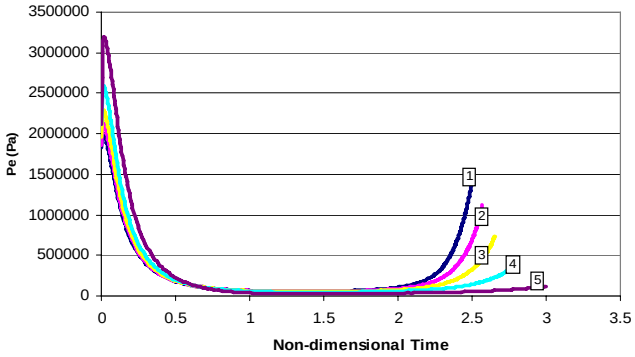

Figure 16: Pressure on the Aluminum plate surface at r=0 versus Non-dimensional time in the cases of: (1) H*=0.05 (2) H*=0.005 (3) H*=0.0025 (4) H*=0.0015 (5) H*=0.001

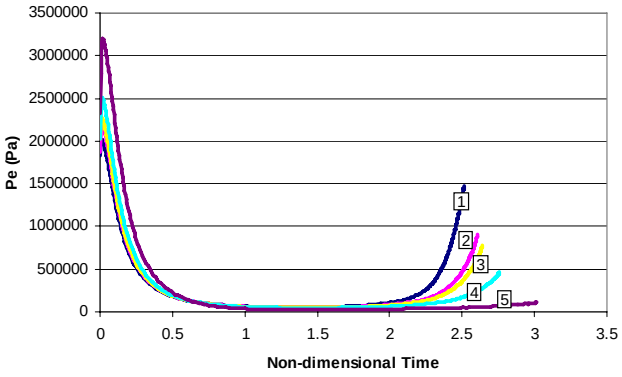

Figure 17: Pressure on the Magnesium plate surface at r=0 versus Non-dimensional time in the cases of: (1) H*=0.05 (2) H*=0.005 (3) H*=0.004 (4) H*=0.0025 (5) H*=0.0015

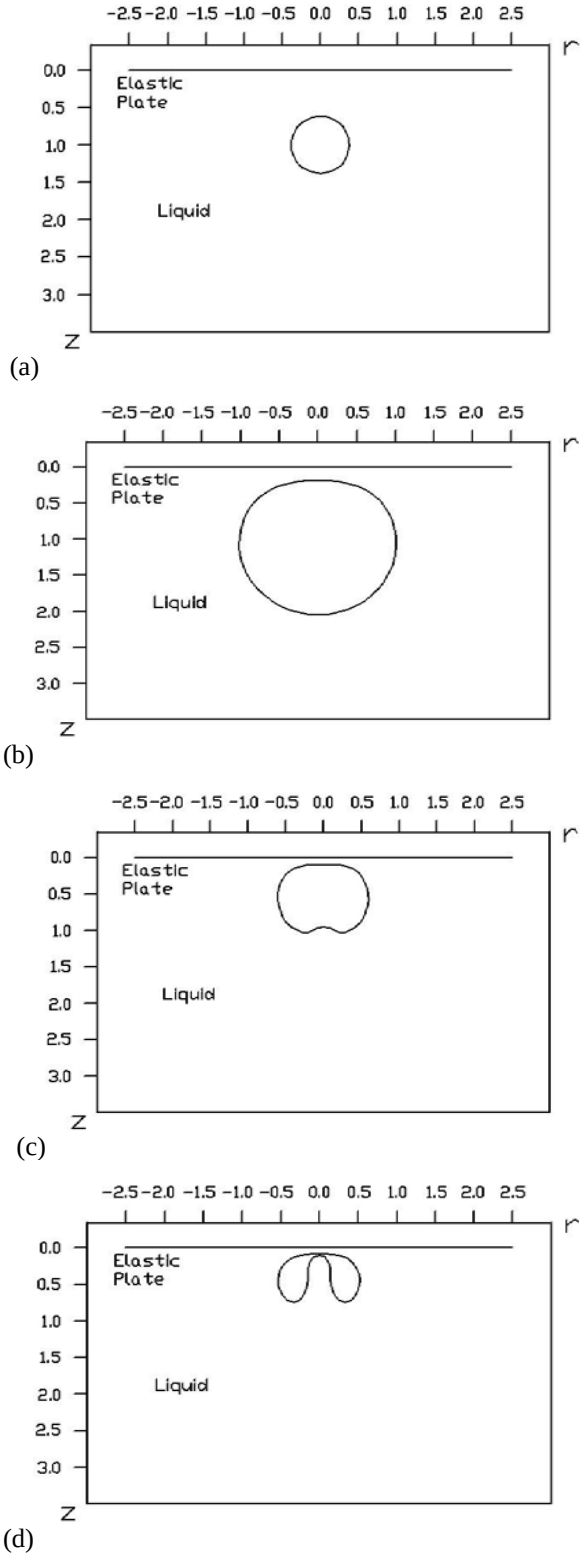

Figure 18: Time dependent profiles of a high energy input generated vapor bubble near a thin Steel plate with non-dimensional thickness of H*=0.005. The corresponding non-dimensional times are: (a) 0.00273 (b) 1.30557 (c) 2.38048 (d) 2.52296

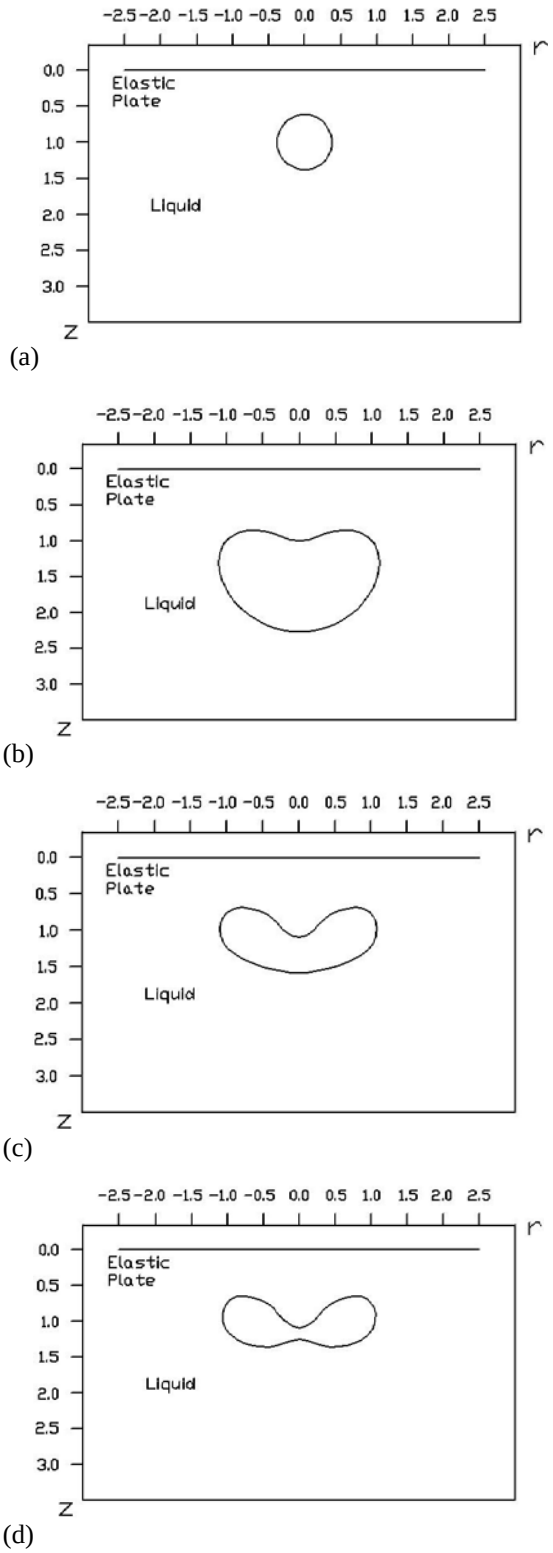

Figure 19: Time dependent profiles of a high energy input generated vapor bubble near a thin Steel plate with non-dimensional thickness of H*=0.00035. The corresponding non-dimensional times are: (a) 0.00273 (b) 1.77304 (c) 2.78231 (d) 2.98147

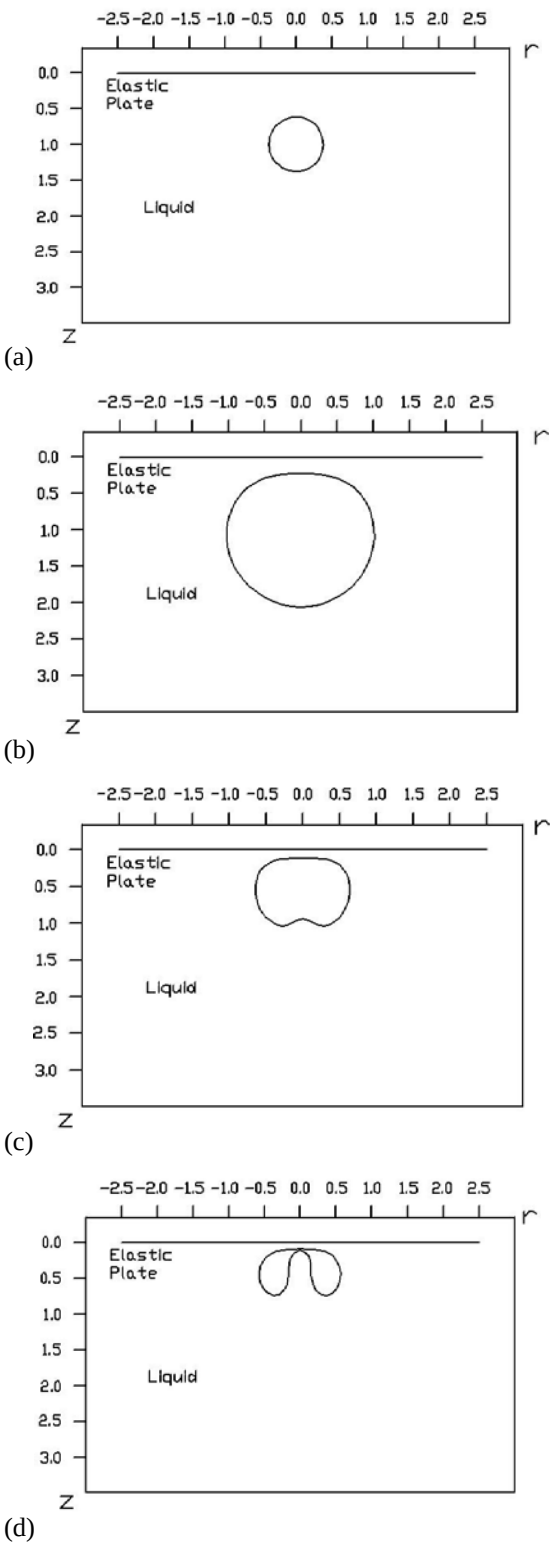

Figure 20: Time dependent profiles of a high energy input generated vapor bubble near a thin aluminum plate with non-dimensional thickness of H*=0.005. The corresponding non-dimensional times are: (a) 0.00273 (b) 1.32934 (c) 2.415561 (d) 2.5677

Figure 18 shows the successive profiles of the vapor bubble near a thin steel plate with non-dimensional thickness of H*=0.005. In this figure it is shown that the liquid micro jet is directed towards the elastic plate.
Figure 19 shows the successive profiles of the vapor bubble near a thin steel plate with non-dimensional thickness of H*=0.00035. In this figure it is shown that the minute displacement of the thin steel plate affects the dynamic behavior of the bubble and the liquid micro jet is directed away from the elastic plate.

Figure 20 shows the successive profiles of the vapor bubble near a thin aluminum plate with non-dimensional thickness of H*=0.005. In this figure it is shown that the liquid micro jet is directed towards the elastic plate.
Figure 21 shows the successive profiles of the vapor bubble near a thin aluminum plate with non-dimensional thickness of H*=0.001. In this figure it is shown that the minute displacement of the thin aluminum plate affects the dynamic behavior of the bubble and the liquid micro jet is directed away from the elastic plate.

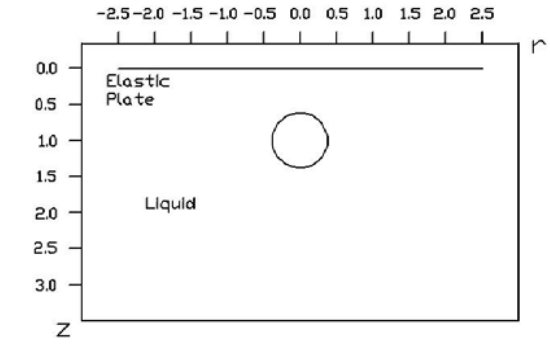

(a)

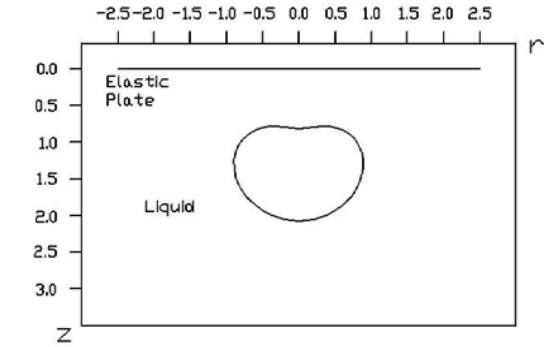

(b)

Figure 21

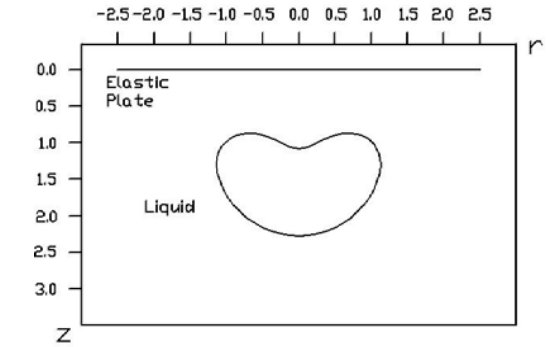

(c)

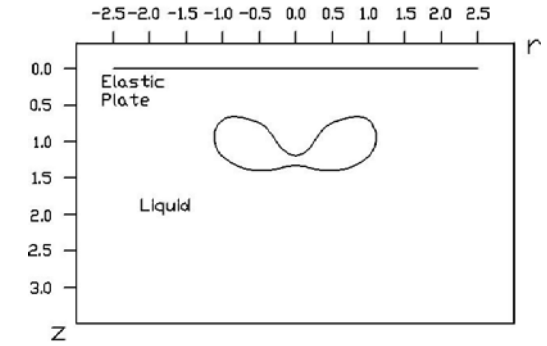

(d)

Figure 21: Time dependent profiles of a high energy input generated vapor bubble near a thin aluminum plate with non-dimensional thickness of H*=0.001. The corresponding non-dimensional times are: (a) 0.00273 (b) 1.82179 (c) 2.80103 (d) 2.9975

Figure 22 shows the successive profiles of the vapor bubble near a thin magnesium plate with non-dimensional thickness of H*=0.005. In this figure it is shown that the liquid micro jet is directed towards the elastic plate.
Figure 23 shows the successive profiles of the vapor bubble near a thin magnesium plate with non-dimensional thickness of H*=0.0015. In this figure it is shown that the minute displacement of the thin magnesium plate affects the dynamic behavior of the bubble and the liquid micro jet is directed away from the elastic plate.

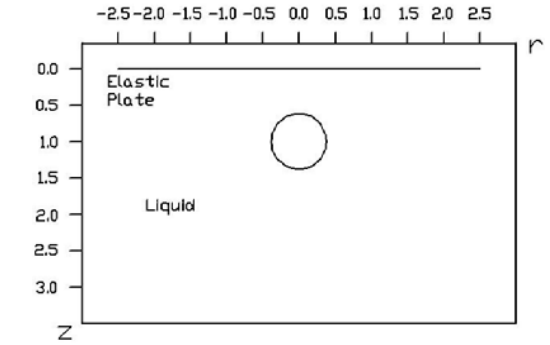

(a)

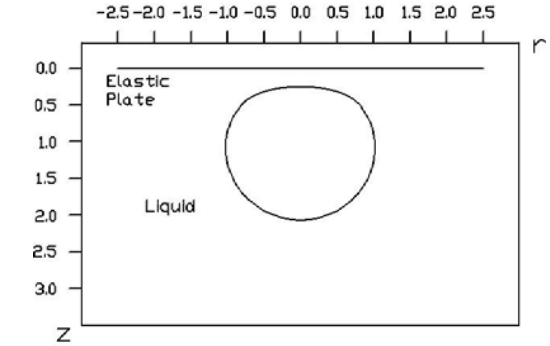

(b)

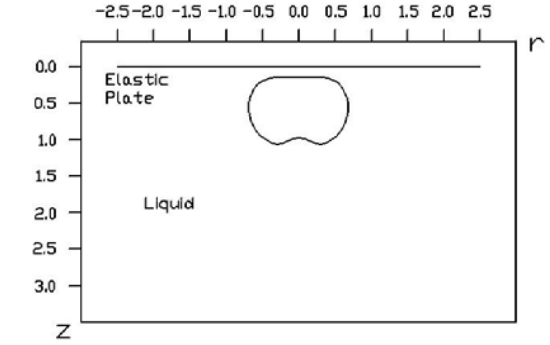

(c)

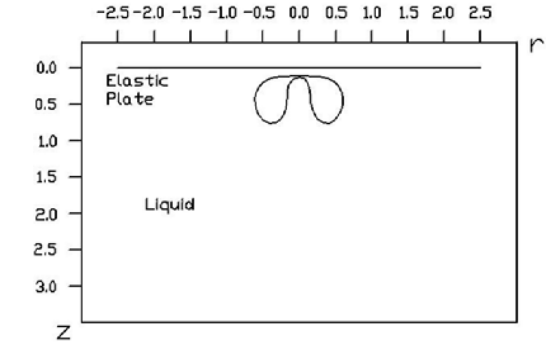

(d)

Figure 22: Time dependent profiles of a high energy input generated vapor bubble near a thin magnesium plate with non-dimensional thickness of H*=0.005. The corresponding non-dimensional times are: (a) 0.00273 (b) 1.35525 (c) 2.44623 (d) 2.6063

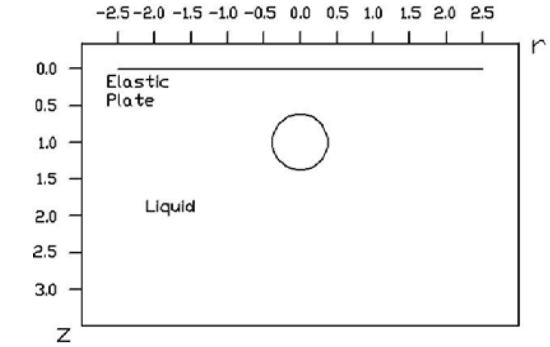

(a)

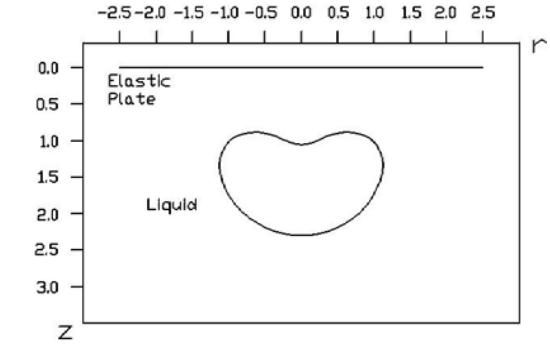

(b)

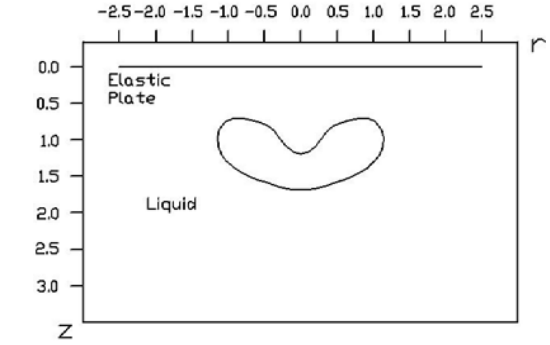

(c)

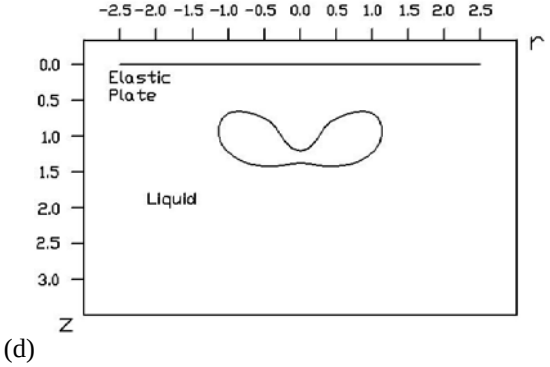

(d)

Figure 23: Time dependent profiles of a high energy input generated vapor bubble near a thin magnesium plate with non-dimensional thickness of H*=0.0015. The corresponding non-dimensional times are: (a) 0.00273 (b) 1.84396 (c) 2.81071 (d) 3.01625

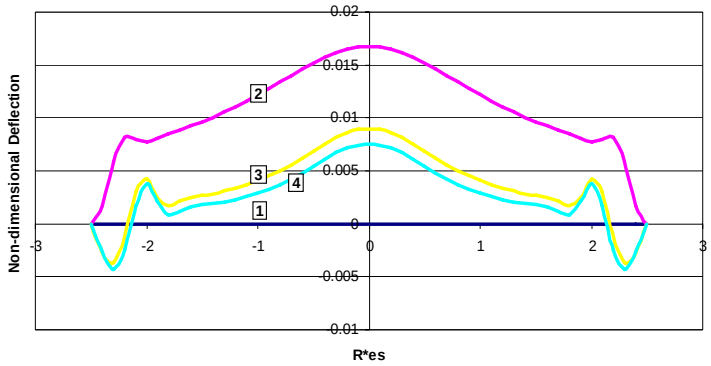

Figure 24: Non-dimensional deflection of the Steel plate with H*=0.005 in non-dimensional times of: (1) t*=0.00273 (2) t*=1.30557 (3) t*= 2.38048 (4) t*=2.52296

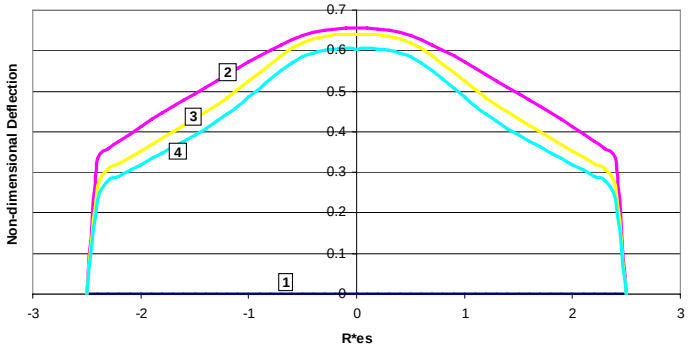

Figure 25: Non-dimensional deflection of the Steel plate with H*=0.00035 in non-dimensional times of:: (1) 0.00273 (2) 1.77304 (3) 2.78231 (4) 2.98147

Figures 24 and 25 illustrare the non-dimensional deflection of the thin steel plate during the pulsation of a vapor bubble in its vicinity in different non-dimensional times. These figures show that by decreasing the thicknss of the thin metal plate, the deflection of its centre point increases.

CONCLUSION

Results show that during the growth and collapse of a vapor bubble near a thin elastic plate with a proper thickness and flexural rigidity, in the absence of strong buoyancy forces, a liquid micro jet may develop on the closest side of the bubble to the thin elastic plate and directed away from it. The results also show that the minute displacement of the elastic surface has significant effect on the behavior of the nearby collapsing bubble.

NOMENCLATURE

P_∞	Pressure in the far field
P_c	Saturated vapour pressure
P_b	Variable pressure inside the bubble
R	Radius of the bubble
R_{ES}	Radius of the elastic plate
R_0	Initial small radius
R_m	Maximum radius of the bubble
Δr	Radial distance between nodes on the surface
ϕ	Velocity potential
$\psi = \frac{\partial \phi}{\partial n}$	Normal velocity of the boundary
u_j	Radial velocity of each element on the surface of the bubble
v_j	Vertical velocity of each element on the surface of the bubble
η	Tangential velocity
g	Gravity acceleration
w	Vertical displacement of the plate
ρ	Mass per unit area of the plate
ρ_l	Mass per unit area of the liquid
H	Thickness of the plate
D	Flexural rigidity of the plate
E	Elastic module of the plate
ν	Poissons' ratio
h	Initial distance of the bubble centroid from the thin elastic plate
$\Phi = \frac{\phi}{R_m}\left(\frac{\rho}{P_\infty - P_C}\right)^{\frac{1}{2}}$	Non-dimensional velocity potential
$\Delta t^* = \frac{\Delta t}{R_m}\left(\frac{P_\infty - P_C}{\rho}\right)^{\frac{1}{2}}$	Non-dimensional Time
$P^* = \frac{P - P_C}{P_\infty - P_C}$	Non-dimensional Pressure on the surface of the plate
$E^* = \frac{E}{P_\infty - P_C}$	Non dimensional Elastic Module
$H^* = \frac{H}{R_m}$	Non-dimensional Thickness of the plate
$R^* = \frac{r}{R_m}$	Non-dimensional radius of the bubble
$Z^* = \frac{Z}{R_m}$	Non-dimensional vertical coordinate
$r^* = \frac{r}{R_m}$	Non-dimensional radial coordinate
$R^*_{es} = \frac{R_{ES}}{R_m}$	Non-dimensional radius of the plate

$$\gamma = \frac{h}{R_m}$$ Stand-off parameter

REFERENCES

[1] Blake, J. R. & Gibson, D. C. (1987) " Cavitation bubbles near boundaries". *Ann. Rev. Fluid Mech.* 19 pp. 99-123.

[2] Blake, J. R., Robinson, P. B., Shima, A. & Tomita, Y. (1993) "Interaction of two cavitation bubbles with a rigid boundary". *J. Fluid Mech.* 255, 707-721.

[3] Blake, J. R., Hotton, M. C., Robinson, P. B. & Tong, R. P. (1997) "Collapsing cavities, toroidal bubbles and jet impact". *Phil.Trans. R. soc. Lond.* A 355 pp. 537-550.

[4] Benjamin, T. B. & Ellis, A. T. (1966) "The collapse of cavitation bubble and the pressure thereby produced against solid boundaries". *Phil.Trans. R. soc. Lond.* A 260 pp. 221-240.

[5] Brujan, E. A., Nahen, k., Schmidt, P. &Vogel, A. (2001) "Dynamic of laser-induced cavitation bubbles near elastic boundaries: Influence of the elastic modulus". *J. Fluid Mech.* 443 pp. 283-314.

[6] Brujan, E. A., Nahen, k., Schmidt, P. &Vogel, A. (2001) "Dynamic of laser-induced cavitation bubbles near an elastic boundary". *J. Fluid Mech.* 433 pp. 251-281.

[7] Gibson, D. C. & Blake, J. R. (1980) "Growth and collapse cavitation bubble near flexible boundaries'. In Proc. 7 th Australian Conf. on Hydraulics and Fluid Mechanics, Brisbane, pp. 283-286. The institution of engineers, Australia.

[8] Duncan, J.H & Zhang, s., (1991) "On the interaction of a collapsing cavity and a compliant wall." J. Fluid Mech. 226 pp. 401-423.

[9] Best, J. P. (1991) "The dynamic of underwater explosions". Phd Thesis. University of Wollogong, Wollongong, Australia.

[10] Rayleigh, Lord (1917) "On the pressure developed in a liquid during collapse of a spherical void". *Phil Mag* 34 pp. 94-98.

[11] Love, AEH. (1927), "A treatise on the mathematical theory of elasticity" Cambridge university press, Cambridge.

[12] Shervani-Tabar, M. T. (1995), "Computer study of a cavity bubble near a rigid boundary, a free surface and a compliant wall" PhD Thesis, University of Wollongong, Wollongong, Australia.